

Transport in Bilayer Graphene: Calculations within a self-consistent Born approximation

Mikito Koshino and Tsuneya Ando

Department of Physics, Tokyo Institute of Technology 2-12-1 Ookayama, Meguro-ku, Tokyo 152-8551, Japan

(Dated: November 26, 2024)

The transport properties of a bilayer graphene are studied theoretically within a self-consistent Born approximation. The electronic spectrum is composed of k -linear dispersion in the low-energy region and k -square dispersion as in an ordinary two-dimensional metal at high energy, leading to a crossover between different behaviors in the conductivity on changing the Fermi energy or disorder strengths. We find that the conductivity approaches $2e^2/\pi^2\hbar$ per spin in the strong-disorder regime, independently of the short- or long-range disorder.

I. INTRODUCTION

Recently there was an experimental development in fabrication of atomically thin graphene, or single-layer graphite, that enables us to access its exotic electronic properties.^{1,2,3} The magnetotransport was measured and the integer quantum Hall effect was observed.^{4,5,6} In the experiments, a multilayer that contains a few graphene sheets is also available.^{4,6} The electronic structure of a bilayer graphene was studied theoretically and the spectrum was found to be essentially different from that of a monolayer.⁷ The purpose of this paper is to study transport properties of the bilayer graphene.

A graphite monolayer has a k -linear, massless Dirac-like spectrum and has long attracted theoretical interests as a “relativistic” problem in condensed matter physics, where k is the absolute value of the wave vector. Theoretical studies of transport in such an exotic electronic structure have been given by several authors, where the conductivity with or without magnetic field,^{8,9} the Hall effect,^{10,11} quantum corrections to the conductivity,¹² and the dynamical transport¹³ are investigated. The results show that the conductivity exhibits various singular behaviors in the vicinity of zero energy.^{8,10,13,14,15,16}

In bilayer graphene the energy dispersion includes both k -linear and k -square terms. In this paper, we calculate the diagonal conductivity in the absence of a magnetic field within a self-consistent Born approximation (SCBA). A similar SCBA analysis has been applied for monolayer graphene.^{8,10,13} We shall find that the coexistence of k -linear and k -square dispersions leads to a crossover between transport properties similar to those of a monolayer graphene and to those of an ordinary two-dimensional metal as the Fermi energy is changed. The conductivity becomes nearly universal, $2e^2/\pi^2\hbar$ per spin, in the case of large disorder. The analysis is made for two different kinds of scatterers, short range and long range, where the former represents on-site random energies distributed on the carbon atoms and the latter a slowly varying random potential of the range much longer than the lattice constant but shorter than the typical electron wavelength.

In Sec. II, the effective Hamiltonian and the resulting energy spectrum in a bilayer graphene are discussed, and

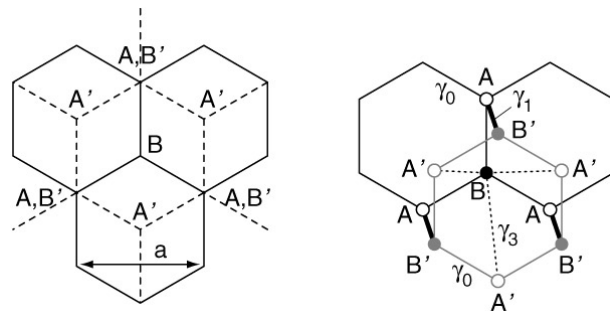


FIG. 1: (Left) Top view of the atomic structure in a bilayer graphene. Solid and dashed lines represent the top (A and B sites) and bottom layers (A' and B' sites), respectively. (Right) Definition of the hopping parameters in a tight-binding model, γ_0 between nearest-neighbor sites in each layer, γ_1 between A and B' , and γ_3 between B and A' .

model scatterers are introduced. The self-consistent Born approximation is briefly described in Sec. III. Explicit results are discussed for short-range scatterers in Sec. IV and for long-range scatterers in Sec. V. A discussion and a brief summary are given in Sec. VI.

II. EFFECTIVE HAMILTONIAN AND ENERGY SPECTRUM

The bilayer graphene is composed of a pair of hexagonal networks of carbon atoms, which include A and B atoms on the top layer and A' and B' on the bottom, as schematically shown in Fig. 1. The two layers are arranged in AB stacking, where A atoms are located above B' atoms, and B or A' atoms are above or below the center of hexagons in the other layers. The unit cell contains four atoms A , B , A' , and B' , and the Brillouin zone becomes identical with that of the monolayer graphene. We model the system by a tight-binding Hamiltonian based on the Slonczewski-Weiss-McClure graphite model.^{17,18} We include three parameters γ_0 , γ_1 , and γ_3 , where γ_0 represents the intralayer coupling $A \leftrightarrow B$ or $A' \leftrightarrow B'$, and γ_1 and γ_3 the interlayer coupling $A \leftrightarrow B'$ and $B \leftrightarrow A'$, respectively. The coupling parameters are estimated as

$\gamma_0 \approx 3.16$ eV,¹⁹ $\gamma_1 \approx 0.39$ eV,²⁰ and $\gamma_3 \approx 0.315$ eV.²¹

We can show that the low energy spectrum is given by the states around the K and K' points in the Brillouin zone. Neighboring A and B' sites are coupled by γ_1 to create the bonding and antibonding states away from the Fermi level, and the low energy states are given by the remaining A' and B sites.⁷ The effective Hamiltonian reads,

$$\mathcal{H}_K = \frac{\hbar^2}{2m^*} \begin{pmatrix} 0 & k_-^2 \\ k_+^2 & 0 \end{pmatrix} - \frac{\hbar^2 k_0}{2m^*} \begin{pmatrix} 0 & k_+ \\ k_- & 0 \end{pmatrix}, \quad (1)$$

$$\mathcal{H}_{K'} = \frac{\hbar^2}{2m^*} \begin{pmatrix} 0 & k_+^2 \\ k_-^2 & 0 \end{pmatrix} + \frac{\hbar^2 k_0}{2m^*} \begin{pmatrix} 0 & k_- \\ k_+ & 0 \end{pmatrix}, \quad (2)$$

where $k_{\pm} = k_x \pm ik_y$ with \mathbf{k} being the wave vector measured from the K or K' points, and the effective mass m^* and the wave number k_0 defined by

$$\frac{\hbar^2}{2m^*} = \frac{(\sqrt{3}a\gamma_0/2)^2}{\gamma_1}, \quad (3)$$

and

$$k_0 = \frac{2}{\sqrt{3}a} \frac{\gamma_3\gamma_1}{\gamma_0^2}, \quad (4)$$

with the lattice constant $a = 0.246$ nm. The k -linear term in the Hamiltonian (2) describes the direct hopping between A' and B sites, and the k -square term the second-order process between A' and B via A - B' dimers. A typical energy where the k -square and k -linear terms become comparable can be defined by

$$\varepsilon_0 = \frac{\hbar^2 k_0^2}{2m^*} = \left(\frac{\gamma_3}{\gamma_0} \right)^2 \gamma_1. \quad (5)$$

The eigenenergy of (2) becomes

$$\varepsilon_{j\mathbf{k}s} = \frac{\hbar^2}{2m^*} s k \sqrt{k^2 \mp 2k_0 k \cos 3\varphi + k_0^2}, \quad (6)$$

where the upper sign corresponds to $j = K$ and the lower to K' , $s = \pm 1$, $k = \sqrt{k_x^2 + k_y^2}$, and $\varphi = \arg(k_+)$ with $\arg(z)$ being the argument φ in $z = |z|e^{i\varphi}$. The eigenvectors corresponding to (6) are

$$\phi^{j\mathbf{k}s} = \begin{pmatrix} \phi_{A'}^{j\mathbf{k}s} \\ \phi_B^{j\mathbf{k}s} \end{pmatrix} = \frac{1}{\sqrt{2}} \begin{pmatrix} e^{i\theta_{j\mathbf{k}}} \\ s \end{pmatrix}, \quad (7)$$

with

$$\theta_{K\mathbf{k}} = \arg(-k_0 e^{i\varphi} + k e^{-2i\varphi}), \quad (8)$$

$$\theta_{K'\mathbf{k}} = \arg(k_0 e^{-i\varphi} + k e^{2i\varphi}). \quad (9)$$

Figure 2 shows the energy dispersion (6) for $j = K$. In the high-energy region $|\varepsilon| > (1/4)\varepsilon_0$, we have a single trigonally warped Fermi line, which becomes closer to a circle on going to the higher energy as the k -square term dominates in the Hamiltonian. The equienergy line

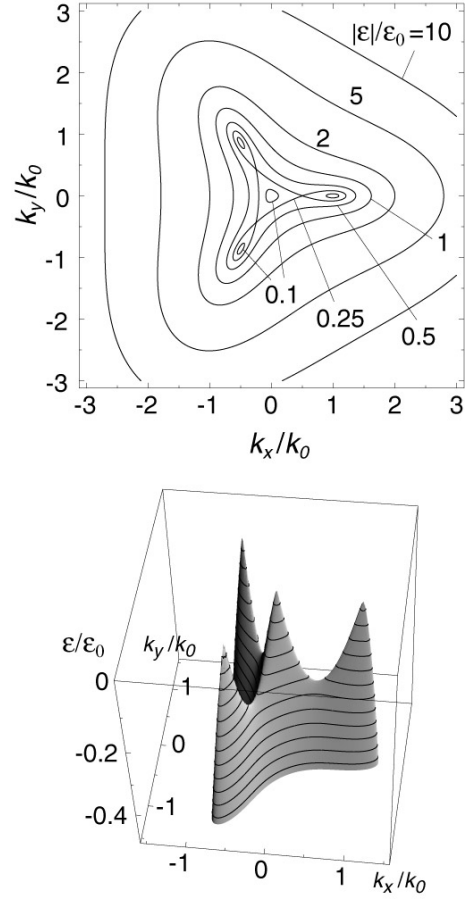


FIG. 2: Equienergy lines (top) and the three-dimensional plot (bottom) of the energy dispersion of the bilayer graphene around the K point. In the latter only the lower half ($\varepsilon < 0$) is shown.

becomes convex for $\varepsilon \gtrsim 10.8\varepsilon_0$. In the low-energy region $|\varepsilon| < (1/4)\varepsilon_0$, the Fermi line splits into four separate pockets for each of K and K' , one center part and three satellite parts that are located trigonally. In the vicinity of zero energy $|\varepsilon| \ll \varepsilon_0$, the dispersion becomes linear in k space with respect to the four Fermi points, where the center pockets can be approximated as a circle with radius $k = |\varepsilon/\varepsilon_0|k_0$ and the three satellites as ellipses with the longer and shorter radii $|\varepsilon/\varepsilon_0|k_0$ and $|\varepsilon/\varepsilon_0|k_0/3$. While splitting of the four Fermi lines occurs only at very low energies, the trigonal warping extends to much higher energy as seen in Fig. 2.

The velocity operator $v_x = (\partial\mathcal{H}/\partial k_x)/\hbar$ has nonzero matrix elements between the states on the identical k points (j, \mathbf{k}) written as

$$(v_{j\mathbf{k}})_{ss'} \equiv \langle j\mathbf{k}s' | v_x | j\mathbf{k}s \rangle = s w_{j\mathbf{k}} + s' w_{j\mathbf{k}}^*, \quad (10)$$

with

$$w_{K\mathbf{k}} = \frac{\hbar}{4m^*} (-k_0 + 2k e^{-i\varphi}) e^{-i\theta_{K\mathbf{k}}}, \quad (11)$$

$$w_{K'\mathbf{k}} = \frac{\hbar}{4m^*}(k_0 + 2ke^{i\varphi})e^{-i\theta_{K'\mathbf{k}}}. \quad (12)$$

In the high-energy region $|\varepsilon| > (1/4)\varepsilon_0$, the mean square velocity averaged on the contour $\varepsilon = |\varepsilon_{j\mathbf{k}s}|$ is given by

$$\langle |(v_{j\mathbf{k}})_{ss'}|^2 \rangle_\varepsilon = \frac{|\varepsilon|}{m^*} + \frac{\varepsilon_0}{2m^*}(1 + ss'), \quad (13)$$

where the first and second terms come from the k -square and k -linear terms in the dispersion, respectively. In the vicinity of zero energy $|\varepsilon| \ll \varepsilon_0$, we have

$$\langle |(v_{j\mathbf{k}})_{ss'}|^2 \rangle_\varepsilon = \frac{3\varepsilon_0}{4m^*}. \quad (14)$$

The density of states per spin is defined by

$$\rho_0(\varepsilon) = \frac{1}{\Omega} \sum_{j\mathbf{k}s} \delta(\varepsilon - \varepsilon_{j\mathbf{k}s}), \quad (15)$$

where Ω is the area of the system. In the high energy region $|\varepsilon| > (1/4)\varepsilon_0$, this becomes

$$\rho_0(\varepsilon) \approx \frac{m^*}{\pi\hbar^2} \equiv \rho_\infty, \quad (16)$$

with terms of the order of $O(\varepsilon_0^2/\varepsilon^2)$ neglected. In the vicinity of zero energy $|\varepsilon| \ll \varepsilon_0$, on the other hand,

$$\rho_0(\varepsilon) \approx \frac{4m^*}{\pi\hbar^2} \frac{|\varepsilon|}{\varepsilon_0}. \quad (17)$$

The density of states diverges logarithmically at $|\varepsilon|/\varepsilon_0 = 1/4$ due to the presence of saddle points in the dispersion.

For the parameters mentioned above, $m^*/m_0 = 0.033$ with m_0 being the free-electron mass, $k_0(2\pi/a)^{-1} = 2.2 \times 10^{-3}$, and $\varepsilon_0 \approx 3.9$ meV. The electron concentration corresponding to $(1/4)\varepsilon_0$ is $n_s = 1.7 \times 10^{10} \text{ cm}^{-2}$, that to ε_0 is $1.0 \times 10^{11} \text{ cm}^{-2}$, and that to $10.8\varepsilon_0$ is $1.1 \times 10^{12} \text{ cm}^{-2}$. As the typical electron concentration in the present system is 10^{12} cm^{-2} ($\varepsilon/\varepsilon_0 \sim 10$) or larger,⁶ the trigonal warping is appreciable, but it is extremely hard to realize the situation where four Fermi lines are well split from each other.

The Hamiltonian (2) is formally equivalent to that of the monolayer system, where the k -square term comes from a higher-order term in the $\mathbf{k} \cdot \mathbf{p}$ approximation.²² However, the parameter ε_0 for the monolayer becomes the order of γ_0 and thus is larger than in the bilayer by the order of 1000, and the k -square term gives only a small perturbation. In the bilayer, on the contrary, the k -square term becomes dominant in the dispersion at small energy ε_0 . Note also that the Hamiltonian (2) becomes invalid when the energy becomes as high as the anti-bonding states of the A - B' dimers. The deviation from (2) seems to become appreciable around $\varepsilon \sim \gamma_1/4$ (~ 0.1 eV corresponding to $n_s \sim 2.7 \times 10^{12} \text{ cm}^{-2}$).⁷ The dispersion of the bilayer graphene is much closer to that of three-dimensional graphite, where we see a similar trigonal structure in the $k_x - k_y$ plane with a fixed wave number k_z along the stacking direction.^{17,23}

In terms of the eigenvector $\phi^{j\mathbf{k}s}$ the amplitudes of the atomic orbitals at sites $\mathbf{R}^{A'}$ and \mathbf{R}^B are given by

$$\psi_{A'}(\mathbf{R}^{A'}) = \frac{1}{\sqrt{N}} \phi_{A'}^{j\mathbf{k}s} \exp[i(\mathbf{K}_j + \mathbf{k}) \cdot \mathbf{R}^{A'}], \quad (18)$$

$$\psi_B(\mathbf{R}^B) = \frac{\omega_j}{\sqrt{N}} \phi_B^{j\mathbf{k}s} \exp[i(\mathbf{K}_j + \mathbf{k}) \cdot \mathbf{R}^B], \quad (19)$$

for $j = K$ and K' , where $\omega_K = \omega^{-1}$, $\omega_{K'} = \omega$ with $\omega = \exp(2\pi i/3)$, and N is the number of unit cells in the system.

The dominant scatterers in the present system are not well known. In the following, we shall consider two kinds of model scatterers, short-range scatterers localized only on B sites or on A' sites and long-range scatterers, the potential of which spreads over a certain length scale larger than the lattice constant a . In each case we assume that the disorder strength is weaker than the dimer coupling γ_1 , so that we need to consider only the potential on A' and B sites. The effective Hamiltonian for the disorder potential can be derived similarly as in monolayer graphene, if we identify the A' and B sites in the bilayer with A and B in the monolayer.^{24,25}

The matrix elements for the short-ranged potential are written as

$$\begin{aligned} \langle j'\mathbf{k}'s' | U_i^{A'} | j\mathbf{k}s \rangle &= \frac{u_i^A}{\Omega} e^{i(\mathbf{K}_j + \mathbf{k} - \mathbf{K}_{j'} - \mathbf{k}') \cdot \mathbf{R}_i^{A'}} (\phi_{A'}^{j'\mathbf{k}'s'})^* \phi_{A'}^{j\mathbf{k}s}, \end{aligned} \quad (20)$$

$$\begin{aligned} \langle j'\mathbf{k}'s' | U_i^B | j\mathbf{k}s \rangle &= \frac{u_i^B}{\Omega} e^{i(\mathbf{K}_j + \mathbf{k} - \mathbf{K}_{j'} - \mathbf{k}') \cdot \mathbf{R}_i^B} (\omega_j \phi_B^{j'\mathbf{k}'s'})^* \omega_j \phi_B^{j\mathbf{k}s}, \end{aligned} \quad (21)$$

for scatterers at $\mathbf{R}_i^{A'}$ and \mathbf{R}_i^B , respectively, where u_i^A and u_i^B are the integrated intensities of the potential, i.e., the coefficient of the δ potential. For long range disorder, we assume that the potential range is much larger than the lattice constant a but smaller than the typical wavelength $2\pi/k$ with k being the wave number from the K or K' point. Then we can neglect the matrix elements for intervalley scatterings between K and K' , while those for intravalley can be written as

$$\langle j'\mathbf{k}'s' | U_i | j\mathbf{k}s \rangle = \delta_{jj'} \frac{u_i}{\Omega} e^{i(\mathbf{k} - \mathbf{k}') \cdot \mathbf{R}_i} (\phi^{j'\mathbf{k}'s'})^\dagger \phi^{j\mathbf{k}s}, \quad (22)$$

where u_i is the integrated intensity of the potential.

We have another possibility for the long-range disorder potential, where each of the scatterers is effective only in one layer. This is modeled by a long-range potential that has amplitude only over either A' or B sites. The situation then becomes almost equivalent to the short-range case, the only difference being that K and K' are decoupled, reducing the self-energy by a factor of 2.

III. SELF-CONSISTENT BORN APPROXIMATION

In the self-consistent Born approximation, the self-energy of the disorder-averaged Green's function $\langle G_{\alpha,\alpha'} \rangle$

is given by⁸

$$\Sigma_{\alpha,\alpha'}(\varepsilon) = \sum_{\alpha_1,\alpha'_1} \langle U_{\alpha,\alpha_1} U_{\alpha'_1,\alpha'} \rangle \langle G_{\alpha_1,\alpha'_1}(\varepsilon) \rangle, \quad (23)$$

with $\alpha = (j\mathbf{k}s)$, where $\langle \ \rangle$ represents the average over the impurity configurations. In the present system the conductivity becomes isotropic in spite of the presence of strong trigonal warping. It can be calculated by the Kubo formula,

$$\sigma(\varepsilon) = \frac{\hbar e^2}{2\pi\Omega} \text{Re Tr} [\langle v_x G^R v_x G^A \rangle - \langle v_x G^R v_x G^R \rangle], \quad (24)$$

where $G^R = (\varepsilon - \mathcal{H} + i0)^{-1}$ and $G^A = (\varepsilon - \mathcal{H} - i0)^{-1}$ are the retarded and the advanced Green's functions, respectively, with \mathcal{H} being the Hamiltonian including the disorder potential. This can be rewritten as

$$\sigma(\varepsilon) = \frac{\hbar e^2}{2\pi\Omega} \text{Re Tr} [v_x \langle G^R \rangle \tilde{v}_x^{RA} \langle G^A \rangle - v_x \langle G^R \rangle \tilde{v}_x^{RR} \langle G^R \rangle], \quad (25)$$

with $\tilde{v}_x^{RA} = \tilde{v}_x(\varepsilon + i0, \varepsilon - i0)$ and $\tilde{v}_x^{RR} = \tilde{v}_x(\varepsilon + i0, \varepsilon + i0)$ satisfying

$$\tilde{v}_x(\varepsilon, \varepsilon') = v_x + \langle UG(\varepsilon)\tilde{v}_xG(\varepsilon')U \rangle. \quad (26)$$

In the SCBA, \tilde{v}_x should be calculated in the ladder approximation. In the above and hereafter we omit the summation over the spin degeneracy, so the actual conductivity should be multiplied by a factor of 2.

In the case of the present model scatterers, the self-energy and therefore the averaged Green's function become diagonal with respect to the wave number and the band index. Further, the self-energy is independent of the wave number and the band index, and thus is determined by the energy alone. As a result we have

$$\langle G_{\alpha,\alpha'}(\varepsilon) \rangle = \delta_{\alpha,\alpha'} G_{\alpha}(\varepsilon), \quad (27)$$

$$G_{\alpha}(\varepsilon) = G(\varepsilon, \varepsilon_{\alpha}) \equiv \frac{1}{\varepsilon - \Sigma(\varepsilon) - \varepsilon_{\alpha}}, \quad (28)$$

where $\Sigma(\varepsilon)$ is the self-energy.

IV. SHORT-RANGE SCATTERERS

For short-range scatterers, we assume that they are equally distributed to A and B sites with density $n_i^A = n_i^B = n_i/2$ and the identical mean square amplitude $\langle (u_i^A)^2 \rangle = \langle (u_i^B)^2 \rangle = u^2$. Then, the self-energy is given by

$$\Sigma(\varepsilon) = \frac{n_i u^2}{4\Omega} \sum_{\alpha} G_{\alpha}(\varepsilon). \quad (29)$$

By substituting the summation over j and \mathbf{k} with the integration in energy $\varepsilon' = |\varepsilon_{j\mathbf{k}s}|$, we can rewrite this as

$$\Sigma(\varepsilon) = \frac{n_i u^2}{4} \int_0^{\infty} d\varepsilon' \rho_0(\varepsilon') \sum_s G(\varepsilon, s\varepsilon'). \quad (30)$$

The density of states is given by

$$\rho(\varepsilon) = -\frac{1}{\pi\Omega} \sum_{\alpha} \text{Im} G_{\alpha}(\varepsilon + i0) = -\frac{4}{\pi n_i u^2} \text{Im} \Sigma(\varepsilon + i0). \quad (31)$$

For the conductivity, we can show that the vertex correction vanishes in the short-range scatterers, or $\tilde{v}_x = v_x$, and we obtain

$$\begin{aligned} \sigma(\varepsilon) &= \frac{\hbar e^2}{2\pi\Omega} \text{Re} \sum_{j\mathbf{k}ss'} |(v_{j\mathbf{k}})_{ss'}|^2 (G_{j\mathbf{k}s}^R G_{j\mathbf{k}s'}^A - G_{j\mathbf{k}s}^R G_{j\mathbf{k}s'}^R) \\ &= \frac{\hbar e^2}{2\pi} \int_0^{\infty} d\varepsilon' \rho_0(\varepsilon') \sum_{ss'} \langle |(v_{j\mathbf{k}})_{ss'}|^2 \rangle_{\varepsilon'} \\ &\quad \times \text{Re} [G(\varepsilon + i0, s\varepsilon') G(\varepsilon - i0, s'\varepsilon') \\ &\quad - G(\varepsilon + i0, s\varepsilon') G(\varepsilon + i0, s'\varepsilon')]. \end{aligned} \quad (32)$$

In the second equality we have replaced the summation over j and \mathbf{k} with the integral in $\varepsilon' = |\varepsilon_{j\mathbf{k}s}|$.

We first look at the Boltzmann limit by taking $\Sigma \rightarrow 0$, which should be valid in the weak-disorder case satisfying $|\varepsilon| \gg |\Sigma|$. By assuming that Σ is infinitesimal in (30), we can calculate Σ explicitly as

$$\Sigma(\varepsilon + i0) = -i \frac{\pi}{2} W \varepsilon_0 \frac{\rho_0(\varepsilon)}{\rho_{\infty}} \equiv -i \frac{\hbar}{2\tau}, \quad (33)$$

where τ is the lifetime and the dimensionless parameter W is defined by

$$W = \frac{n_i u^2}{2} \frac{\rho_{\infty}}{\varepsilon_0}. \quad (34)$$

For sufficiently high energy, $\hbar/2\tau \approx (\pi/2)\varepsilon_0 W$ showing that $W \sim 1$ characterizes a typical disorder strength that smears out the fine low-energy structure due to the k -linear term. This W is the same as that defined for a monolayer graphene in Ref. 13 and as A^{-1} in Ref. 8.

For the conductivity, we take only the terms with $G^R G^A$ and $s = s'$ as a dominant contribution in (32), and obtain a familiar form,

$$\sigma(\varepsilon) \approx e^2 \rho_0 \tau \langle v_x^2 \rangle_{\varepsilon}. \quad (35)$$

Here $\langle v_x^2 \rangle_{\varepsilon} = \langle |(v_{j\mathbf{k}})_{ss}|^2 \rangle_{\varepsilon}$ is the Fermi-surface average of the diagonal matrix element of v_x and use has been made of the approximation

$$\frac{1}{\Omega} \sum_{\alpha} G_{\alpha}^R(\varepsilon) G_{\alpha}^A(\varepsilon) \approx \frac{2\pi\tau}{\hbar} \rho_0. \quad (36)$$

With the use of (13) the conductivity for the higher energy $|\varepsilon| > \varepsilon_0$ becomes

$$\sigma(\varepsilon) = \frac{e^2}{\pi^2 \hbar} \frac{1}{W} \left(\frac{|\varepsilon|}{\varepsilon_0} + 1 \right). \quad (37)$$

The term proportional to $|\varepsilon|$ results from the k -square term of the dispersion and is rewritten as $e^2 \rho_{\infty} |\varepsilon| \tau / m^*$

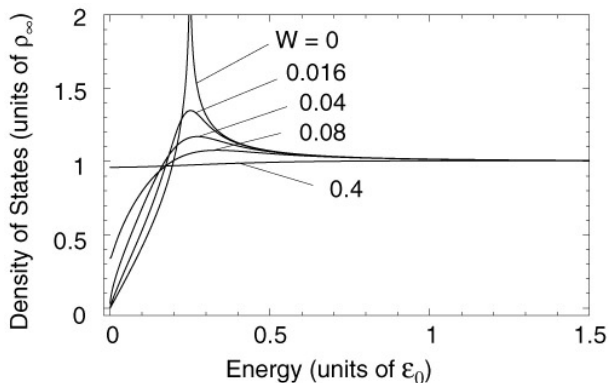


FIG. 3: Density of states per spin calculated in the SCBA. Plots become identical for the short- and long-range scatterers.

as in the usual two-dimensional metal. The term independent of $|\varepsilon|$ is a correction due to the trigonal warping caused by the k -linear term, which never vanishes even as $\varepsilon \rightarrow \infty$. In the low-energy region $|\varepsilon| \ll \varepsilon_0$, we have

$$\sigma(\varepsilon) = \frac{e^2}{\pi^2 \hbar} \frac{3}{4W}. \quad (38)$$

The energy-independent conductivity is essentially the same as that of monolayer graphene.⁸

In the case of large disorder $W > 1$, the fine structure in the density of states disappears completely (see below) and therefore the imaginary part of the self-energy becomes independent of energy and the real part becomes negligible. Thus, we always have

$$\Sigma(\varepsilon + i0) \approx -i\Gamma, \quad (39)$$

with

$$\Gamma = \frac{\pi}{2} W \varepsilon_0, \quad (40)$$

giving

$$\rho(\varepsilon) \approx \rho_\infty. \quad (41)$$

We can calculate the conductivity (32) by substituting the high-energy expansions (13) and (16), and obtain

$$\sigma(\varepsilon) \approx \frac{e^2}{\pi^2 \hbar} [S(\varepsilon) + 1] + \frac{e^2}{\pi^2 \hbar} \frac{1}{W}, \quad (42)$$

with

$$S(\varepsilon) = \left(\frac{\varepsilon}{\Gamma} + \frac{\Gamma}{\varepsilon} \right) \arctan \frac{\varepsilon}{\Gamma}, \quad (43)$$

where terms of the order of $O(1/W^2)$ are neglected. The first term of (42) comes from the k -square term in the dispersion and the second term is a correction due to the k -linear term.

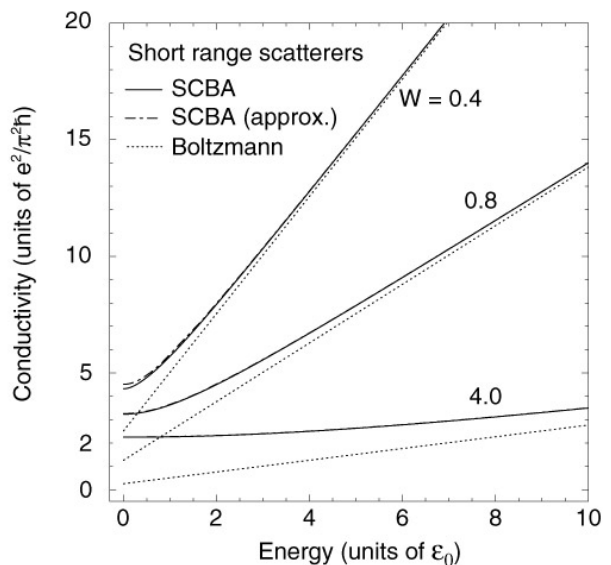
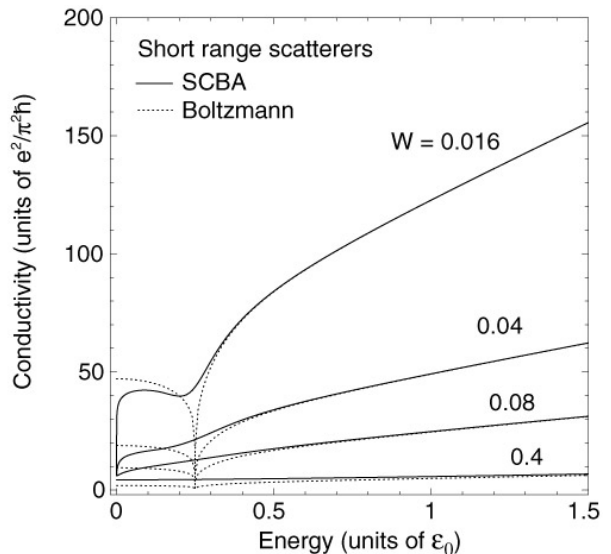


FIG. 4: Calculated SCBA conductivity (solid) and Boltzmann conductivity (dotted) per spin in the case of short-range disorder, with upper and lower panels showing smaller and larger W 's. For the Boltzmann conductivity in the lower panel we used the expression (37) which is valid for $\varepsilon > \varepsilon_0$. In the lower panel the approximate result given by Eq. (42) is also shown.

The conductivity goes to the Boltzmann limit (37) for $\varepsilon > \Gamma$, while for $\varepsilon < \Gamma$ it becomes

$$\sigma = \frac{e^2}{\pi^2 \hbar} \left(2 + \frac{1}{W} \right). \quad (44)$$

It is interesting that the conductivity becomes universal, i.e., $\sigma \rightarrow 2e^2/\pi^2 \hbar$, and never vanishes in the limit of the large disorder. At a rough estimate, we can derive this expression by putting the uncertainty relation $\varepsilon \sim \Gamma$ in (37). In Sec. VI, this universal conductivity will be reconsidered in terms of Einstein's relation.

The self-consistent equation (30) can be solved easily by a numerical iteration. Figure 3 shows the density of states calculated for several disorder strengths. We notice that the logarithmic divergence present in $\rho_0(\varepsilon)$ at $\varepsilon/\varepsilon_0 = 1/4$ is smeared out very easily, and the structure in the vicinity of $\varepsilon = 0$ due to the k -linear dispersion disappears around $W \sim 0.1$ and is almost unrecognizable already for $W = 0.4$.

The corresponding plot for the conductivity is shown in Fig. 4 along with the Boltzmann limit. In weak disorder $W \ll 1$ we observe a sharp dip at zero energy. This is the analog of monolayer graphene,⁸ showing that k -linear dispersion around zero energy remains intact at small disorder. Further discussion of the asymptotic value at $\varepsilon = 0$ will be given in Sec. VI. The Boltzmann conductivity drops to zero at $|\varepsilon| = (1/4)\varepsilon_0$, as the velocity vanishes at the saddle points in the dispersion, but this singularity disappears due to the finite density of states. Apart from this difference the results are almost the same as those in the Boltzmann limit. The conductivities for large W 's are plotted in a different scale in the lower panel in Fig. 4, compared with the high-energy expression of the Boltzmann limit (37) and the approximate expression (42). The curves deviate from the Boltzmann limit in the region $\varepsilon < \Gamma$ and never fall below $2e^2/(\pi^2\hbar)$ even in strong disorder. The analytic expression becomes valid already for $W \sim 1/2$.

V. LONG-RANGE SCATTERERS

For the long-range disorder, we consider scatterers with density n_i and mean square amplitude $\langle (u_i)^2 \rangle = u^2$. The two valleys K and K' are now decoupled and the conductivity is written as the summation of their individual contributions. The self-energy is given by

$$\Sigma(\varepsilon) = \frac{n_i u^2}{2\Omega} \sum_{\mathbf{k}s} G_{j\mathbf{k}s}(\varepsilon), \quad (45)$$

which differs from (29) for short-range disorder in that the prefactor is larger by a factor of 2 and that the summation is taken only in one valley. However those two elements cancel and the self-energy becomes identical with (30) in this notation. We can omit the valley index j completely.

The conductivity without the vertex correction, denoted by σ^0 , is equivalent to (32). The vertex part (26) is given by

$$\begin{aligned} \langle j\mathbf{k}s' | \tilde{v}_x(\varepsilon, \varepsilon') | j\mathbf{k}s \rangle &= \langle j\mathbf{k}s' | v_x | j\mathbf{k}s \rangle \\ &+ \frac{\hbar k_0}{4m^*} \frac{B(\varepsilon, \varepsilon')}{1 - \Pi(\varepsilon, \varepsilon')} (s e^{-i\theta_{j\mathbf{k}}} + s' e^{i\theta_{j\mathbf{k}}}), \end{aligned} \quad (46)$$

where Π and B are dimensionless quantities defined by

$$\Pi(\varepsilon, \varepsilon') = \frac{n_i u^2}{4\Omega} \sum_{\mathbf{k}} \sum_{ss'} G_{j\mathbf{k}s}(\varepsilon) G_{j\mathbf{k}s'}(\varepsilon'), \quad (47)$$

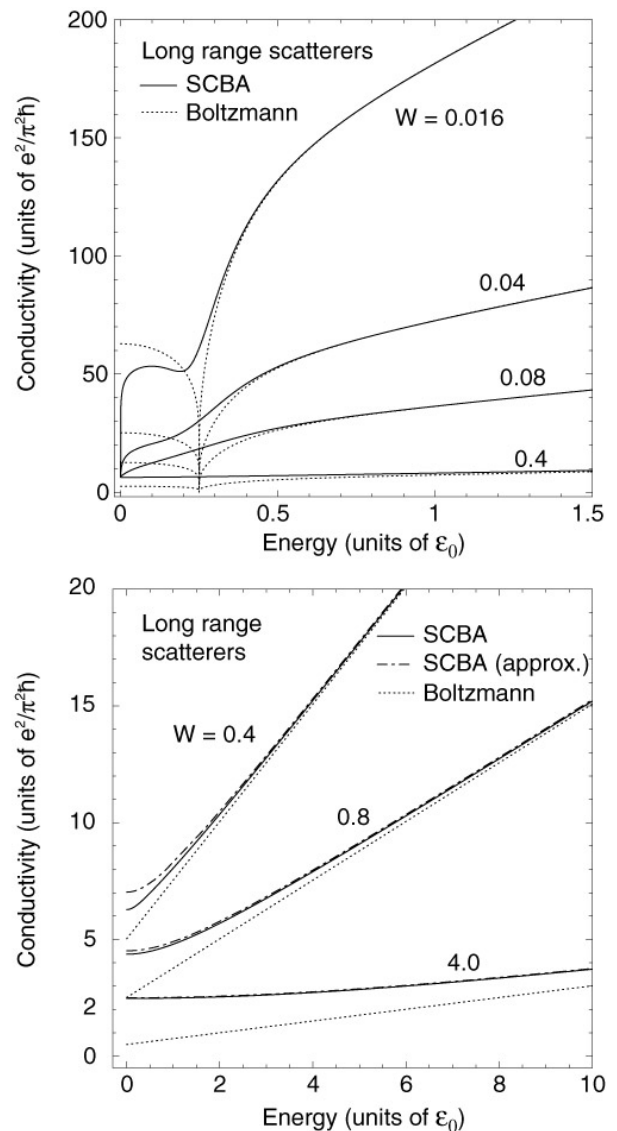


FIG. 5: Calculated SCBA conductivity (solid) and Boltzmann conductivity (dotted) per spin in the case of long-range disorder, with upper and the lower panel showing smaller and larger W 's, respectively. For the Boltzmann conductivity in the lower panel we used the expression in (52) which is valid for $\varepsilon > \varepsilon_0$. In the lower panel the approximate result given by Eq. (53) is also shown.

$$B(\varepsilon, \varepsilon') = \frac{n_i u^2}{4\Omega} \sum_{\mathbf{k}} \sum_{ss'} [1 + ss' \text{Re}(\tilde{w}_{j\mathbf{k}} e^{-i\theta_{j\mathbf{k}}})] \times G_{j\mathbf{k}s}(\varepsilon) G_{j\mathbf{k}s'}(\varepsilon'), \quad (48)$$

with $\tilde{w}_{j\mathbf{k}} = w_{j\mathbf{k}}(\hbar k_0/4m^*)^{-1}$. The conductivity correction including the valley degeneracy is then written as

$$\delta\sigma(\varepsilon) = \frac{e^2}{\pi^2\hbar} \frac{1}{2W} \text{Re} \left(\frac{(B^{RA})^2}{1 - \Pi^{RA}} - \frac{(B^{RR})^2}{1 - \Pi^{RR}} \right), \quad (49)$$

where $B^{RA} = B(\varepsilon+i0, \varepsilon-i0)$ and $B^{RR} = B(\varepsilon+i0, \varepsilon+i0)$.

In the Boltzmann limit, only the term including B^{RA} and Π^{RA} is relevant. A straightforward calculation gives

$$\Pi^{RA} = \frac{1}{2}, \quad (50)$$

$$B^{RA} = \frac{1}{2} \langle 1 + \text{Re}(\tilde{w}_{j\mathbf{k}} e^{-i\theta_{j\mathbf{k}}}) \rangle_{\varepsilon}. \quad (51)$$

We can easily show that $\langle \text{Re}(\tilde{w}_{j\mathbf{k}} e^{-i\theta_{j\mathbf{k}}}) \rangle_{\varepsilon} = 1$ to obtain $\delta\sigma/(e^2/\pi^2\hbar) = 1/W$ in the limit $\varepsilon > \varepsilon_0$. In the case $\varepsilon \ll \varepsilon_0$, on the other hand, $\langle \text{Re}(\tilde{w}_{j\mathbf{k}} e^{-i\theta_{j\mathbf{k}}}) \rangle_{\varepsilon} = 0$ and therefore $\delta\sigma/(e^2/\pi^2\hbar) = 1/4W$. The total conductivity combined with σ^0 in (37) or (38) becomes

$$\sigma(\varepsilon) = \begin{cases} \frac{e^2}{\pi^2\hbar} \frac{1}{W} \left(\frac{|\varepsilon|}{\varepsilon_0} + 2 \right) & (\varepsilon > \varepsilon_0), \\ \frac{e^2}{\pi^2\hbar} \frac{1}{W} & (\varepsilon \ll \varepsilon_0). \end{cases} \quad (52)$$

In the case of large disorder $W > 1$, we can derive the analytic expression similarly to the short-range case. By using the self-energy (39) we can show that $B_{RA} = 1$, $B_{RR} = 0$, and $\Pi_{RA} = 1/2$, giving the vertex correction $\delta\sigma(\varepsilon) = (e^2/\pi^2\hbar)/W$ independent of energy. The total conductivity including σ^0 in (42) is written as

$$\sigma(\varepsilon) = \frac{e^2}{\pi^2\hbar} [S(\varepsilon) + 1] + \frac{e^2}{\pi^2\hbar} \frac{2}{W}. \quad (53)$$

For $\varepsilon < \Gamma$, this reduces to

$$\sigma = \frac{e^2}{\pi^2\hbar} \left(2 + \frac{2}{W} \right). \quad (54)$$

The conductivity is given by a universal value as in the short-range case in the limit of large disorder.

We show in Fig. 5 the conductivity numerically computed for the several W 's. The difference from the result in the short-range case is appreciable only in the clean limit $W \ll 1$, because the vertex correction gives only a shift of the order of $(e^2/\hbar)/W$. The conductivity again approaches $2e^2/(\pi^2\hbar)$ in the region $\varepsilon < \Gamma$ in strong disorder. The approximate result (54) is valid for $W \gtrsim 0.8$.

VI. DISCUSSION AND CONCLUSION

In Secs. IV and V we have seen that the conductivity in the case of strong disorder $W > 1$ deviates greatly from the Boltzmann conductivity and converges to the order of $2e^2/\pi^2\hbar$. This can be understood in terms of Einstein's relation

$$\sigma = e^2 \rho D^*, \quad (55)$$

with the density of states ρ and the diffusion constant D^* . The diffusion constant is written as $D^* = \langle v_x^2 \rangle \tau$, where $\langle v_x^2 \rangle$ is the average of the squared velocity over states at the Fermi energy and τ is a relaxation time related to Γ through the uncertainty relation $\Gamma = \hbar/2\tau$.

If we neglect the k -linear term in the dispersion, we have $\langle v_x^2 \rangle = |\varepsilon|/m^*$ and therefore $\sigma = n_s e^2 \tau / m^*$ with $n_s = \rho_{\infty} |\varepsilon|$. This is nothing but the Boltzmann conductivity for $|\varepsilon| \gg \Gamma$. In the energy range $|\varepsilon| < \Gamma$, however, we have $\langle v_x^2 \rangle \sim \Gamma/m^*$ because we take an average over the states $\varepsilon_{\alpha} \lesssim \Gamma$. Thus, the diffusion constant becomes $D^* \sim \hbar/2m^*$ independent of energy using $\Gamma\tau \sim \hbar/2$. Upon using $\rho = \rho_{\infty} = m^*/\pi\hbar^2$, the conductivity becomes $\sigma \sim e^2/\hbar$. This conductivity is universal and independent of the band parameters and the strength of scattering. It is also independent of short- or long-range disorder.

The situation becomes different in the weak-disorder limit $W \ll 1$, where σ at zero energy drops from the Boltzmann conductivity almost by the factor W . This behavior is essentially equivalent to that in monolayer graphene, where the conductivity drops from the Boltzmann to the universal value $e^2/\pi^2\hbar$ in the vicinity of the zero energy and the near-singular drop was ascribed to a reduction of the effective density of states contributing to the conductivity.⁸ The universal value was shown to be unaffected by magnetic fields,⁸ and similar near-singular behavior was shown to be present in various transport quantities.^{13,14,15} A universal conductivity at zero energy was also reported in the square tight-binding lattice model with one-half flux,¹⁶ which has k -linear dispersion as well.

This zero-energy conductivity can be explicitly estimated from (32) with the density of states (17) and the square velocity (14). The integral turns out to be independent of the imaginary part of the self-energy and returns a universal value

$$\sigma(0) = \frac{6e^2}{\pi^2\hbar}, \quad (56)$$

which is six times as large as the conductivity in the monolayer. The extra factor comes from the product of the density of states and the square velocity, $3|\varepsilon|/(\pi\hbar^2)$, which is larger than in the monolayer by a factor of 6 due to the existence of the satellite elliptic Fermi pockets.

Recently transport properties of bilayer graphene were studied experimentally.⁶ The resistivity exhibits a prominent peak at $\varepsilon \approx 0$ and decreases rapidly with the increase of the energy or the electron concentration. This dependence is explained by Eq. (42) or (53) (or the lower panel of Fig. 4 or 5) qualitatively quite well with the disorder parameter $1 \lesssim W \lesssim 2$, in the region $n_s \lesssim 2 \times 10^{12} \text{ cm}^{-2}$. In particular, the observed peak resistivity $\sim 6.5 \text{ k}\Omega$ corresponds well to the present result for $W \sim 2$ in the case of long-range disorder (dominant usually) and $W \sim 1$ in the case of short-range disorder. However, the observed resistivity seems to decrease much faster than that given by Eq. (42) or (53) with a constant W for larger electron concentrations $n_s \gtrsim 2 \times 10^{12} \text{ cm}^{-2}$. This might suggest that the effective range of the scattering potential can be comparable to the electron wavelength at these electron concentrations.

We have studied the quantum transport in bilayer graphene in zero magnetic field with the self-consistent

Born approximation. The coexistence of the k -linear and k -square dispersion is observed as two different behaviors in the Boltzmann conductivity, like that in the usual two-dimensional metal and in a monolayer graphene with a massless Dirac spectrum, which are energetically separated. The conductivity in the SCBA deviates from the Boltzmann limit in the case of strong disorder $W \gtrsim 1$, and converges to $\sim 2e^2/(\pi^2\hbar)$ (per spin). The conductivity in the long-range scatterers exhibits a qualitatively similar behavior to that in the short-range case, while the vertex correction gives a positive shift of the order of $1/W$.

ACKNOWLEDGMENTS

This work has been supported in part by the 21st Century COE Program at Tokyo Tech “Nanometer-Scale Quantum Physics” and by Grants-in-Aid for Scientific Research from the Ministry of Education, Culture, Sports, Science and Technology, Japan. Numerical calculations were performed in part using the facilities of the Supercomputer Center, Institute for Solid State Physics, University of Tokyo.

-
- ¹ K. S. Novoselov, A. K. Geim, S. V. Morozov, D. Jiang, Y. Zhang, S. V. Dubonos, I. V. Grigorieva, and A. A. Firsov, *Science* **306**, 666 (2004).
- ² C. Berger, Z. Song, T. Li, X. Li, A. Y. Ogbazghi, R. Feng, Z. Dai, A. N. Marchenkov, E. H. Conrad, P. N. First, and W. A. de Heer, *J. Phys. Chem. B* **108**, 19912 (2004).
- ³ Y. Zhang, J. P. Small, W. V. Pontius, and P. Kim, *Appl. Phys. Lett.* **86**, 073104 (2005).
- ⁴ K. S. Novoselov, A. K. Geim, S. V. Morozov, D. Jiang, M. I. Katsnelson, I. V. Grigorieva, S. V. Dubonos, and A. A. Firsov, *Nature* **438**, 197 (2005).
- ⁵ Y. Zhang, Y. W. Tan, H. L. Stormer, and P. Kim, *Nature* **438**, 201 (2005).
- ⁶ K. S. Novoselov, E. McCann, S. V. Morozov, V. I. Fal'ko, M. I. Katsnelson, U. Zeitler, D. Jiang, F. Schedin, and A. K. Geim, *Nat. Phys.* **2**, 177 (2006).
- ⁷ E. McCann and V. I. Fal'ko, *Phys. Rev. Lett.* **96**, 086805 (2006).
- ⁸ N. H. Shon and T. Ando, *J. Phys. Soc. Jpn.* **67**, 2421 (1998).
- ⁹ N. M. R. Peres, A. H. Castro Neto, and F. Guinea, *cond-mat/0512476*.
- ¹⁰ Y. Zheng and T. Ando, *Phys. Rev. B* **65**, 245420 (2002).
- ¹¹ V. P. Gusynin and S. G. Sharapov, *Phys. Rev. Lett.* **95**, 146801 (2005).
- ¹² H. Suzuura and T. Ando, *Phys. Rev. Lett.* **89**, 266603 (2002); *J. Phys. Soc. Jpn.* **72** Suppl. A, 69 (2003).
- ¹³ T. Ando, Y. Zheng, and H. Suzuura, *J. Phys. Soc. Jpn.* **71**, 1318 (2002).
- ¹⁴ T. Ando and H. Suzuura, *Physica E* **18**, 202 (2003).
- ¹⁵ T. Ando, *Solid State Commun.* **12**, 69 (2003); *Physica E* **22**, 656 (2004).
- ¹⁶ E. Fradkin, *Phys. Rev. B* **33**, 3257 (1986).
- ¹⁷ J. W. McClure, *Phys. Rev.* **108**, 612 (1957).
- ¹⁸ J. C. Slonczewski and P. R. Weiss, *Phys. Rev.* **109**, 272 (1958).
- ¹⁹ W. W. Toy, M. S. Dresselhaus and G. Dresselhaus, *Phys. Rev. B* **15**, 4077 (1977).
- ²⁰ A. Misu, E. Mendez, and M. S. Dresselhaus, *J. Phys. Soc. Jpn.* **47**, 199 (1979).
- ²¹ R. E. Doezema, W. R. Datars, H. Schaber, and A. Van Schyndel, *Phys. Rev. B* **19**, 4224 (1979).
- ²² H. Ajiki and T. Ando *J. Phys. Soc. Jpn.* **65**, 505 (1996).
- ²³ J. -C. Charlier, X. Gonze, and J. -P. Michenaud, *Phys. Rev. B* **43**, 4579 (1991).
- ²⁴ T. Ando and T. Nakanishi, *J. Phys. Soc. Jpn.* **67**, 1704 (1998).
- ²⁵ T. Ando, *J. Phys. Soc. Jpn.* **74**, 777 (2005).